Sena-Cruz, J.M.; Barros, J.A.O.; Coelho, M.R.; Silva, L. (2011) "Efficiency of different techniques in flexural strengthening of RC beams under monotonic and fatigue loading." Construction & Building Materials. (DOI: 10.1016/j.conbuildmat.2011.10.044)

EFFICIENCY OF DIFFERENT TECHNIQUES IN FLEXURAL STRENGTHENING OF RC BEAMS UNDER MONOTONIC AND FATIGUE LOADING

José M. Sena-Cruz[1,2], Joaquim A. O. Barros[1,3], Mário R. F. Coelho[1,4], Luís F. F. T. Silva[1,5]

[1] ISISE, Univ. of Minho, Dept. of Civil Engineering, Campus de Azurém, 4810-058 Guimarães, Portugal.

[2] E-mail: jsena@civil.uminho.pt; ***Corresponding author***

[3] E-mail: barros@civil.uminho.pt

[4] E-mail: mcoelho@civil.uminho.pt

[5] E-mail: luis_t_silva@hotmail.com

Abstract: In the context of flexural strengthening of concrete structures, fiber reinforced polymers (FRP) have been used mostly by two main techniques: *Externally Bonded Reinforcement* (EBR) and *Near-Surface Mounted* (NSM). Both strengthening techniques are applied on the cover concrete, which is normally the weakest region of the element to be strengthened. Consequently, the most common problem is the premature failure of the strengthening system that occurs more frequently in the EBR one. In an attempt of overcoming this weakness, another technique has been proposed, called MF-EBR – *Mechanically Fastened and Externally Bonded Reinforcement*, which uses multi-directional carbon fiber laminates, simultaneously glued and anchored to concrete. To compare the efficiency of NSM, EBR and MF-EBR techniques, four-point bending tests with RC beams were carried out under monotonic and cyclic loading. In this work the tests are described in detail and the obtained results are discussed. Additionally, to assess the performance of a FEM-based computer program for the prediction of the behaviour of RC beams strengthening according to these techniques, the beams submitted to monotonic loading were numerically simulated.

Keywords: flexural strengthening; NSM; EBR; reinforced concrete beams; fatigue; FEM modelling.

1. Introduction

Over the last two decades, extensive research has been developed on the strengthening of reinforced concrete (RC) structures with fiber reinforced polymer (FRP) materials. High stiffness and tensile strength, low weight, easy installation procedures, high durability (no corrosion), electromagnetic permeability and practically unlimited availability in terms of geometry and size are the main advantages of these composites [1, 2].

The most common techniques for applying FRP's are, in general, based on the use of unidirectional FRP's through the: (i) application of fabrics (in situ cured systems) or laminates (pre-cured systems) glued externally on the surface of the element to strengthen (EBR – Externally Bonded Reinforcement); (ii) insertion of laminates (or rods) into grooves opened on the concrete cover (NSM – Near-Surface Mounted) [2, 3]. Epoxy adhesives are the most used to fix the FRP to concrete. The strengthening performance of these techniques depends significantly on the resistance of the concrete cover, which is normally the most degraded concrete region in the structure due to its greater exposure to environment conditions. As a result, premature failure of FRP reinforcement can occur and, generally, the full mechanical capacity of the FRP's is not mobilized, mainly when adopting the EBR technique. To avoid this premature failure complements have been applied to the aforementioned strengthening techniques, such as the application of anchor systems composed of steel plates bolted in the ends of the FRP, the use of strapping with FRP fabric or the use of FRP anchor spikes. In addition to the stress concentration that these localized interventions introduce in the elements to strengthen, they require differentiated and time consuming tasks that can compromise the competitiveness of these techniques.

More recently, some FRP-based alternatives for structural strengthening have been proposed [4]. The mechanically fastened fiber reinforced polymer (MF-FRP) technique has been introduced to strengthen concrete structures, and is mainly characterized by the use of hybrid (carbon and glass) FRP strips that are mechanically fixed to concrete using closely spaced fastening pins and, if necessary, anchors at the ends of the strip are applied to prevent debonding. According to the search performed the MF-FRP concept was initially explored at the University of Wisconsin under supervision of Lawrence Bank in 1998 [4]. This technique has already been used in some applications, e.g. reinforced concrete, wood and masonry structures, and several benefits have been pointed out, namely, quick installation with relatively simple hand tools, no need for special labour skills, no surface preparation required, and the strengthened structure can be immediately used after the installation of the FRP. From these tests an

increase of up to 50% of the carrying capacity was observed in some cases, when compared with the reference structure. Additionally, the occurrence of a more ductile failure mode for the FRP system is referred [5-12]. Nevertheless, some notable disadvantages of this technique have been reported, including greater initial cracking induced by the impact of fasteners in high-strength concrete, and less-effective stress transfer between the FRP and concrete due to the discrete attachment points [13].

Based on the MF-FRP technique, the mechanically fastened and externally bonded reinforcement technique (MF-EBR) has been proposed [14, 15]. The MF-EBR combines the fasteners from the MF-FRP technique and the externally glued properties from the EBR. In addition, all the anchors are pre-stressed. When this strategy is applied high levels of efficacy can be observed.

To assess the efficiency of EBR, NSM and MF-EBR techniques, four-point bending tests with RC beams were carried out under monotonic and fatigue loading. The tests are described and the results are presented and discussed in detail. To appraise the capabilities of a computer program for the prediction of the behaviour of RC beams strengthening according to these techniques, a code package based on the finite element method (FEM) which includes several constitutive models for the material nonlinear analysis of RC structures was applied on the simulation of the beams submitted to monotonic loading.

2. Experimental Program

To appraise the effectiveness of the EBR, MF-EBR and NSM techniques, an experimental program composed of two series of four beams each was carried out. The difference between the series is restricted to the loading configuration: one series was subjected to monotonic loading, while the other to fatigue loading. Each series is composed of a reference beam (REF) and a beam for each investigated strengthening technique.

2.1. Specimens and Test Configuration

The RC beams have a cross section of 200 mm wide and 300 mm height, and 2000 mm of support distance. All the beams have three longitudinal steel bars of 10 mm diameter (3Ø10) at the bottom, and 2Ø10 at the top (see Fig. 1). The transverse reinforcement is composed of steel stirrups of 6 mm diameter (Ø6) with a constant spacing of 100 mm in order to avoid shear failure. Fig. 2 includes the cross section of the strengthened beams.

Table 1 presents the main properties of the beams. In this table t_f, L_f and w_f are the thickness, the length and the width of the laminates, respectively, and $\rho_{s,eq}$ is the equivalent longitudinal steel reinforcement ratio defined by Eq. 1, where b is the width of the beam; A_s and A_f are the cross sectional area of the tensile longitudinal steel bars and FRP systems, respectively; E_s and E_f are the modulus of elasticity of steel and FRP, respectively; and, d_s and d_f are the distance from the top concrete compression fiber to the centroid of the steel bars and FRP systems, respectively. For all the strengthened beams an almost similar $\rho_{s,eq}$ was applied.

$$\rho_{s,eq} = \frac{A_s}{bd_s} + \frac{E_f}{E_s} \cdot \frac{A_f}{bd_f} \quad (1)$$

In this experimental study, a four-point bending test configuration was adopted for the monotonic and fatigue tests (see Fig. 3a). A servo-controlled hydraulic system was used to perform the monotonic tests under displacement control, with a deflection rate of 20 μm/s, using the linear variable differential transducer (LVDT) located at the mid-span of the beam (LVDT3 in Fig. 3).

The fatigue tests were performed between a minimum fatigue level of S_{min}=25% and maximum fatigue level of S_{max}=55%, where the S is the ratio between the applied load and the load carrying capacity, F_m, of the corresponding monotonic beam. According to [2] at 1 million cycles, the fatigue strength of the CFRP material is generally between 60 and 70% of the initial static ultimate strength and is relatively unaffected by the moisture and temperature exposures of concrete structures unless the resin or fiber/resin interface is substantially degraded by the environment. In addition, for the present specimens the yielding of the tensile longitudinal reinforcement start at about S_{max}=60%. Due to these reasons, S_{max} was defined as equal to 55%. The S_{min} was defined taking into account the maximum allowed deflection amplitude that can be applied with the servo-controlled device working at a frequency of 2 Hz. The fatigue tests were composed by three main steps: initially, a monotonic loading was applied under force control at a load rate of 100 N/s up to the maximum level (S_{max}), in order to obtain the initial response of the beam; then, 1 million cycles were imposed at 2 Hz of frequency between $S_{min} \times F_m$ and $S_{max} \times F_m$; finally, a monotonic loading up to the failure, with the same configuration of the monotonic tests, was applied to the beams.

In addition to the LVDT3, four other LVDTs were used to record the deflections in the loaded sections (LVDT2 and LVDT4) and at the sections coinciding with the free end of the FRP systems (LVDT1 and LVDT5), see Fig. 3a. Strain gauges were glued on the longitudinal steel reinforcement and

on the FRPs to measure the strains during the tests, see Fig. 3b-e. The LVDTs had an accuracy of 1.0 μm and a stroke of ±12.5 mm.

2.2. Material Characterization

The mechanical characterization of the concrete was assessed by means of compression tests. For this purpose, six cylindrical concrete specimens were tested at the time of the tested beams to evaluate the compressive strength and the modulus of elasticity according to the recommendations [16] and [17], respectively. From the compression tests, an average compressive strength value of 53.08 MPa, with a coefficient of variation (CoV) of 4.0%, and an average value of 31.17 GPa (CoV=4.4%) for the modulus of elasticity, were obtained. The age of the concrete beams at the date of experimental program was about two years.

The steel of the longitudinal bars and stirrups has a denomination of A400 NR SD according to [18]. The main mechanical properties of these steel bars are presented in the numerical simulation section. Additional information related with the experimental characterization of the steel bars can be found elsewhere [19].

In this work, two different types of CFRP laminates were used: unidirectional (UD-CFRP) for the cases of EBR and NSM techniques, and multi-directional (MDL-CFRP) for the case of the MF-EBR technique. Both laminates have smooth surface. Tensile tests were performed according to [20] for both laminates (UD-CFRP and MDL-CFRP) to assess their tensile properties. Bearing tests with MDL-CFRP specimens were performed, according to [21], to evaluate the bearing resistance of this composite. A detailed description of these tests can be found elsewhere [15]. Table 2 presents the mechanical properties of both laminates. The S&P Resin 220 epoxy adhesive® was used to glue the laminates to the concrete. From the experimental characterization of this adhesive the average values for the following parameters were determined [19]: tensile strength of 33.03 MPa (CoV=8.52%), ultimate strain of 0.48% (CoV=11.80%), modulus of elasticity of 7.47 GPa (CoV=4.28%) . According to the supplier, this epoxy resin has a compressive strength and bond concrete/laminate strength of 90 MPa and 3 MPa, respectively.

A Hilti® chemical anchors system was adopted to fix mechanically the MDL-CFRP laminate to concrete for the case of the MF-EBR beam. This system is composed by the resin HIT-HY 150 max and the HIT-V M8 8.8 threaded anchors.

2.3. Preparation of the Specimens

The preparation of the strengthened beams required several steps. For EBR and NSM beams, the strengthening procedures are quite well documented in the literature [22]. In the case of the MF-EBR beam, its strengthening involved the following main procedures:

a. Holes of 11 mm of diameter and 100 mm depth were made in the soffit of the beam. The holes were cleaned using compressed-air and a steel brush;
b. The holes were filled with the chemical adhesive, and the fasteners were then inserted up to a depth of 100 mm;
c. A rough concrete surface was assured using a rotary hammer with a needle adapter. Compressed-air was used to clean the final surface;
d. A transparent acrylic strip was used to mark the fasteners position and, then, the holes in the laminates were executed. The laminates were cleaned with acetone;
e. Epoxy adhesive was applied on the treated area in the concrete surface and on the laminate surface that will be in contact;
f. The laminate was placed on the concrete surface and pressed against it to create a uniform thickness of 1 to 2 mm;
g. The adhesive in excess was removed and the fasteners were cleaned from any dirt attached;
h. The pre-defined pre-stress level was applied in two phases after the curing time of the epoxy adhesive: a torque moment of 40 N×m was applied to the fasteners one day before the test; in the day of the test, this torque moment was re-installed.

For all the strengthened beams the epoxy adhesive preparation followed the supplier recommendations included in the technical data-sheets. The beams were kept in the laboratory environment before being tested. Tests were carried out at least 7 days after the application of the FRP reinforcement.

From a practical point of view, the holes in the MDL-CFRP should be done after it has been glued to the concrete. However, to minimize the damage in the MDL-CFRP during the concrete drilling process, this strategy was not followed in the present work.

The number of fasteners, the space between them and the depth of the holes were chosen taking into account the information derived from a previous experimental program of direct pull-out bond tests [15].

3. Results

From the results of the performed tests some notes can be taken. In the following paragraphs the main significant aspects are pointed out for the cases of experimental tests and numerical simulations.

3.1. Monotonic Loading Results

Table 3 resumes the main results obtained in the performed tests, while Fig. 4 depicts the relationship between force and displacement at mid-span during the tests. In this table F_{cr}, F_y, and F_{max} are the load at concrete crack initiation, yield initiation of the longitudinal steel bars and maximum load, respectively, and δ_{cr}, δ_y, and δ_{max} are the corresponding vertical displacements at the mid-span; ε_{fu} is ultimate strain in the FRP obtained in tensile tests, whereas ε_{fy} and ε_{fmax} area the maximum strain in the FRP at F_y and F_{max}, respectively.

It can be concluded that the most effective strengthening technique was the MF-EBR, not only due to the maximum load reached (F_{max}=148.2 kN), but also in terms of deflection at failure and ε_{fmax} /ε_{fu} ratio. When compared with the EBR, the MF-EBR system had an increase of the load carrying capacity of about 37%. This superior behaviour cannot be completely explained by the higher axial stiffness, E_fA_f, of the laminate, since the ratio between the E_fA_f of the MDL-CFRP and E_fA_f of the UD-CFRP (used in the EBR beam) is only 1.1. The pre-stressed anchors have contributed for this higher strengthening effectiveness of MF-EBR technique. In fact, while EBR FRP systems failed by FRP peeling, and NSM FRP systems by concrete cover rip-off (detachment of the concrete cover that includes the CFRP strips), the MF-EBR FRP laminates failed by bearing (Fig. 5). The presence of the anchors avoided the premature debonding (peeling) of the laminates, as well as the detachment of the concrete cover (rip-off).

Defining the level of ductility as the ratio between the deflection at the maximum load and the deflection at the yielding of the longitudinal steel bars (δ_{max}/δ_y), in the MF-EBR beam the δ_{max}/δ_y was equal to 4.35, which was much higher than the values registered in the other two strengthened beams, the EBR (1.80) and NSM (2.98) beams.

Apparently, in the MF-EBR beam the force corresponding to the crack initiation, F_{cr}, is higher than the F_{cr} of the other beams. This behaviour can be explained by the contribution of pre-stress. In fact, the pre-stress provided by the anchors may have induced a compressive stress state on the concrete cover, which has delayed the concrete crack initiation. This phenomenon could also explain the higher load

carrying capacity between the concrete crack initiation and the steel yield initiation of the MF-EBR beam. After the longitudinal steel bars have yielded, a slight higher stiffness can be observed in the NSM beam, when compared with the MF-EBR beam. This behaviour can be justified by the confinement that surrounding concrete provides to the NSM CFRP laminates [23].

Fig. 6 presents the strains in the FRP laminates for three distinct load levels: at crack initiation (CR), at yielding initiation of the steel bars (YL), and at the maximum load (UL). In this graph, the location of the strain gauge (SG) is referred to the left extremity of the laminates. As expected, from the extremity of the laminate up to the point load (left shear span length), the strain variation along the laminate increased almost linearly up to the load level corresponding to the yield initiation of the steel bars, which reflects the variation of the applied bending moment. The minimum strains in the MF-EBR laminates up to the yield initiation is justified by the high strain concentration around the fasteners, leading to smaller values in the intermediate zones between consecutive fasteners, where SGf are installed. However, the presence of the fasteners has allowed the development of the highest strain field in the shear span length, which can be justified by analysing the failure mechanism that occurs between two consecutive mechanical fasteners, shown in Figure 7. Due to the concrete compressive struts formed between mechanical fasteners in the shear span region, the laminate bends introducing an increment of strain due to its curvature, which is responsible for the relatively high strain value registered in the SGf2. Due to the highest strain gradient developed near the most external fasteners, and the decrease of the inclination of the concrete struts in the direction of the supports of the beam, a strain value similar to the ones registered in the other strengthening techniques was recorded in SGf1. Since concrete struts were not formed between fasteners in the pure bending zone, the strain registered in the SGF4 is identical to the strain recorded in the EBR technique.

3.2 Fatigue loading

Table 4 includes the relevant results obtained in the post-fatigue monotonic tests, while Fig. 8 depicts the relationship between force and displacement at mid-span up to rupture, after beams having been subjected to one million of cycles.

Up to crack initiation the behaviour of these beams was similar to the one observed in the monotonic tests, i.e. the highest cracking load was registered in the MF-EBR beam. In terms of maximum load and ultimate deflection capacity, the NSM was the most effective strengthening technique. When

compared with the corresponding monotonic tests, marginal variation in terms of maximum load was obtained for the case of the REF, EBR and MF-EBR beams, whereas an increment of 9% was attained in the NSM beam. This might be justified by the smaller number and size of flaws and voids in the adhesive layer that bond the NSM laminates to the concrete of this beam when compared to the NSM monotonic beam. The inferior performance of the MF-EBR beam, when compared with the monotonic one, can be attributed to a possible loss of efficiency of the prestressed anchorages during the fatigue cycles, since only one nut was used per anchor, and due to a bearing strength degradation of the MDL-CFRP during the cycles.

The EBR and NSM beams exhibited the same failure modes occurred in the monotonic tests. Despite the performance in the monotonic tests, the MF-EBR beam presented a more fragile failure mode with bearing and inter-laminar failure of the FRP.

Fig. 9 presents the variation of the minimum and maximum displacements at mid-span during the fatigue cycles. Marginal variations can be observed. In fact, a decrease of 8.3%, 3.0%, 0.3% and 12.1% in terms of stiffness was observed for the REF, EBR, MF-EBR and NSM beams, respectively.
Fig. 9 and a zoom into Fig. 8 show that above the deflection correspondent to the average load between S_{min} and S_{max} in the MF-EBR and NSM beams (≅60kN), a higher degradation of stiffness occurred in the MF-EBR beam. Above this load level the bond effectiveness starts being relevant for the beam's load carrying capacity, which might justify the smaller ultimate load and the corresponding deflection in the MF-EBR beam submitted to fatigue loading. In fact, due to the formation of the concrete struts between consecutive fasteners, with damage to crack formation concentrated near the fasteners (Fig. 5), the bond condition of the MDL-CFRP laminates were degraded during the cyclic loading.

In sections 3.1 and 3.2 several explanations were given for the observed phenomena, but no well supported conclusion can be retrieved due to the small number of tests. Therefore, further investigation is required to verify if the observed tendency is confirmed.

3.3. Numerical simulation

The monotonic tests were numerically simulated. Aspects such as crack initiation, stiffness degradation, steel yield initiation and load carrying capacity are focused. All the simulations were performed with the FEMIX computer program [24]. The tested beams were modelled as a plane stress problem. As example, Fig. 10 shows the geometry, the finite element mesh, loading configuration and support conditions

adopted in the study of the MF-EBR beam. To simulate the concrete part of the specimens, 4-node Serendipity plane stress elements with 2×2 Gauss-Legendre integration scheme were used.

An elasto-plastic multi-fixed smeared crack model was adopted to simulate the nonlinear material behaviour of concrete [25]. The crack evolution in fracture mode I was simulated using the Cornellisen [26] tension softening diagram. The following concrete properties were used in the numerical simulations: density, ρ=25 N/mm^3; Poisson's ratio, ν_c=0.2; initial Young's modulus, E_{ci}=31.17 GPa; compressive strength, f_c= 53.08 MPa; stress at crack initiation, f_{ct}=2.9 MPa; fracture energy, G_c=0.09 N/mm; crack band width, l_b, was assumed equal to square root of the area of the integration point (IP) in order to assure that the results are not dependent of the mesh refinement; threshold angle, α=89º; maximum number of cracks per integration point, n_{cr}=2.

The longitudinal and transverse steel reinforcements, as well as the FRPs, were simulated with 2-node linear cable elements with two Gauss-Legendre integration points. Perfect bond between the concrete and steel reinforcements was assumed. Bi-linear stress-strain relationship up to the ultimate load was assumed for the simulation of steel reinforcements. A linear stress-strain relationship, up to the tensile strength, was adopted for the case of unidirectional laminates (EBR and NSM beams). A bi-linear stress-strain relationship was assumed for the simulation of multi-directional CFRP laminate (MF-EBR beam) to account the bearing behaviour. Table 5 includes the properties adopted in the simulations of the steel reinforcements and FRPs.

Perfect bond between concrete and FRP was assumed for the simulation of the NSM beam since experimental failure mode was by rip-off, while for the cases of EBR and MF-EBR beams slip was allowed. To model slip at the CFRP-concrete interface, in the simulations of EBR and MF-EBR beams 4-node interface finite elements with two Gauss-Lobatto integration points were used. In the present numerical analysis the following relationship in terms of bond stress *versus* slip (τ–s) was adopted to simulate the nonlinear behaviour of the CFRP-concrete interface:

$$\tau(s)=\begin{cases}\tau_m\left(\dfrac{s}{s_m}\right)^{\alpha} & \text{if } s\le s_m\\ \tau_m\left(\dfrac{s}{s_m}\right)^{-\alpha'} & \text{if } s>s_m\end{cases} \qquad (2)$$

where τ_m and s_m are the bond strength and the corresponding slip, respectively; α and α' define the shape of the τ–s law in the pre- and post-peak branches, respectively. Assuming that the normal stiffness of the interface elements has a marginal effect on the bonding behaviour, a constant value of 10^7 N/mm^3 was

attributed. Literature dealing with the bond phenomenon between CFRP's and concrete in the context of MF-EBR technique is extremely scarce. Therefore, the evaluation of τ_m was based on the information included in the technical data-sheet of the adhesive, whereas the other parameters were adjusted to fit the experimental response, mainly s_m, α and α'. Thus, τ_m=3.0 MPa, s_m=0.17 mm, α=0.9 and α'=2.0 were assumed for the simulation of the EBR beam, and τ_m=3.0 MPa, s_m=0.05 mm, α=0.9 and α'=10.0 for the simulation of the MF-EBR beam. To simulate the anchors in the MF-EBR beam, 2-D linear elastic frame elements were used with perfect bond to concrete.

A uniform temperature variation of -146ºC was applied to the frame elements, in order to simulate the pre-stress in anchors (40 N×m torque). With this temperature variation is possible to induce in the anchors the same compressive state that the real torque gives to them.

Fig. 11 depicts the load *versus* deflection at mid-span obtained experimentally and numerically for the REF, EBR, MF-EBR and NSM beams. From the analysis of these curves of the first three beams, the main aspects observed in the experimental tests, such as crack initiation, yield initiation and load carrying capacity are well captured. The numerical simulation of the NSM beam predicts very well the experimental response up to the yield initiation of the steel bars. Above this deflection the model predicts a stiffer response, indicating that after yield initiation this simulation was not able of capturing the intense gradient of damage formed in the concrete surrounding the steel bars and CFRP laminates due to the higher stress transfer gradient to the laminates caused by the yielding of the steel bars.

4. Conclusions

In this paper the flexural strengthening effectiveness of a new technique (MF-EBR) is investigated. This technique combines the fasteners from the MF-FRP technique and the epoxy bond-based performance from the EBR technique. In addition, all the fasteners are pre-stressed. This flexural strengthening technique uses multi-directional laminates exclusively made with carbon fiber reinforced polymers (CFRP).

To compare the efficiency of the MF-EBR, EBR and NSM strengthening techniques, an experimental program with RC beams was carried out. This program is composed by two series of beams, one submitted to monotonic loading and the other to a fatigue loading. In the monotonic tests, when compared to the reference beam, an increase on the loading carrying capacity of 37%, 87% and 86% was obtained for the EBR, MF-EBR and NSM strengthened beams, respectively. When compared to the EBR

beam, an increase of about 37% on the loading carrying capacity for MF-EBR technique was obtained. The most favourable aspect of the MF-EBR technique was, however, the deflection level at ultimate load (δ_{max}), which is an indicator of ductility performance. In fact the normalized deflection capacity at maximum load (δ_{max}/δ_y, with δ_y being the deflection at yield initiation) was 4.35, which was much higher than that registered in the other two strengthened beams, the EBR (1.80) and NSM (2.98) beams. In addition, more ductile failure mode was observed for MF-EBR technique.

In terms of post-fatigue monotonic tests, the NSM beam has provided the highest increase in the ultimate load (101%), since the MF-EBR and EBR beams presented an increase of load capacity of 84% e 43%, respectively, when compared with the maximum load of the control beam. In the fatigue tests the NSM beam presented the highest normalized deflection capacity at maximum load (6.7), while a value of 3.5 and 2.4 was registered in the MF-EBR and EBR beams, respectively.

In spite of the present results being credible, contributing for the knowledge in this area, further investigation is required to better understand the observed phenomena.

Numerical simulations of the monotonic tests demonstrated that current FEM tools can simulate with high accuracy all the principal aspects observed in the tests such as crack initiation, stiffness degradation, yielding initiation in steel bars, and load carrying capacity. However, the smeared crack models hardly capture the rip-off failure mode observed in the NSM beams, since higher gradient of damage formed in the concrete surrounding the steel bars and CFRP laminates occurred.

Acknowledgements

This work is supported by FEDER funds through the Operational Programme for Competitiveness Factors – COMPETE and National Funds through FCT – Portuguese Foundation for Science and Technology under the project PTDC/ECM/74337/2006. The authors acknowledge the materials generously supplied by Hilti Portugal - Productos e Serviços Lda., S&P Clever Reinforcement Ibérica Lda. and SECIL, and TSwaterjet, Lda. for cutting of the laminates using the water-jet technology.

References

[1] Bakis CE, Bank LC, Brown VL, Cosenza E, Davalos JF, Lesko JJ, Machida A, Rizkalla SH, Triantafillou TC. Fiber-Reinforced Polymer Composites for Construction—State-of-the-Art Review. J Compos Construct 2002; 6(2):73-87.

[2] ACI 440F. Guide for the design and construction of externally bonded FRP systems for strengthening concrete structures. Report ACI 440.2R-08. American Concrete Institute, Farmington Hills, USA, 2008, 80 pp.

[3] De Lorenzis L, Teng JG. Near-surface mounted FRP reinforcement: An emerging technique for strengthening structures. Compos Part B 2007; 38(2):119-143.

[4] Bank LC. Mechanically Fastened FRP (MF-FRP) Strips for Strengthening RC Structures – A Viable Alternative. In: Proc. of 2nd International Conference on FRP Composites in Civil Engineering: CICE, Adelaide, Australia, December 8-10, 2004, 12 pp.

[5] Lamanna AJ, Bank LC, Scott DW. Flexural strengthening of reinforced concrete beams using fasteners and fiber-reinforced polymer strips." ACI Struct J 2001; 98(3):368-376.

[6] Lamanna AJ, Bank LC, Scott DW. Flexural strengthening of reinforced concrete beams by mechanically attaching fiber-reinforced polymer strips. J Compos Construct 2004; 8(3):204-209.

[7] Quattlebaum JB, Harries KA, Petrou MF. Comparison of three flexural retrofit systems under monotonic and fatigue loads. J Bridge Eng 2005; 10(6):731-740.

[8] Aidoo J, Harries KA, Petrou MF. Full-scale experimental investigation of repair of reinforced concrete interstate bridge using CFRP materials. J Bridge Eng 2006; 11(3):350-358.

[9] Ekenel M, Rizzo A, Nanny A, Myer JJ. Flexural fatigue behavior of reinforced concrete beams strengthened with FRP fabric and precured laminate systems. J Compos Construct 2006; 10(5):433-442.

[10] Bank LC, Arora D. Analysis of RC beams strengthened with mechanically fastened FRP (MF-FRP) strips. J Compos Struct 2007; 79(2):189-191.

[11] Martin JA, Lamanna AJ. Performance of mechanically fastened FRP strengthened concrete beams in flexure. J Compos Construct 2008; 12(3):257-265.

[12] Lee JH, Lopez MM, Bakis CE. Slip effects in reinforced concrete beams with mechanically fastened FRP strip. J Cement Concrete Compos 2009; 31:496–504.

[13] Ray J C, Scott D W, Lamanna A J, Bank LC. Flexural behavior of reinforced concrete members strengthened using mechanically fastened fiber reinforced polymer plates. In: Proc. 22nd Army Science Conf., United States Army, Washington, D.C., 2000, 556–560.

[14] Micelli F, Rizzo A, Galati D. Anchorage of composite laminates in RC flexural beams. Struct Conc 2010; 11(3):117-126.

[15] Sena-Cruz JM, Barros JAO, Coelho MRF. Bond between concrete and multi-directional CFRP laminates. Adv Mater Res 2010; Vols.133-134:917-922.

[16] NP EN 12390-3:2009. Testing hardened concrete. Part 3: Compressive strength of test specimens.

[17] LNEC E397-1993:1993. Concrete - Determination of the elasticity young modulus under compression. Portuguese specification from LNEC.

[18] NP EN 1992-1-1:2010. Eurocode 2: Design of concrete structures - Part 1-1: General rules and rules for buildings.

[19] Bonaldo E. Composite materials and discrete steel fibers for the strengthening of thin concrete structures. PhD thesis, Dept. of Civil Engineering, Univ. of Minho, September 2008, 404 pp. <http://hdl.handle.net/1822/8842>

[20] ISO 527-4. Plastics - Determination of tensile properties. Part 4: Test conditions for isotropic and orthotropic fiber-reinforced plastic composites. International Organization for Standardization 1997, Genève, Switzerland.

[21] ASTM D 5961/D 5961M-05. Standard test method for bearing response of polymer matrix composite laminates. ASTM International 2005, West Conshohocken, PA.

[22] Barros JAO, Dias SJE, Lima JLT. Efficacy of CFRP-based techniques for the flexural and shear strengthening of concrete beams. J Cement Concrete Compos 2007; 29(3):203-217.

[23] Costa IG, Barros JAO. Assessment of the bond behavior of NSM FRP materials by pullout tests. First Middle East Conference on Smart Monitoring, Assessment and Rehabilitation of Civil Structures, 2011, Dubai.

[24] Sena-Cruz JM, Barros JAO, Azevedo A, Ventura Gouveia A. Numerical simulation of the nonlinear behavior of RC beams strengthened with NSM CFRP strips. CNME 2007-Congress on Numerical Methods in Engineering and XXVIII CILAMCE - Iberian Latin American Congress on Computational Methods in Engineering, 2007, Paper no. 485, FEUP, Porto, 20 pp.

[25] Sena-Cruz, JM. Strengthening of concrete structures with near-surface mounted CFRP laminate strips. PhD thesis, Dept. of Civil Engineering, University of Minho, Portugal, 2004, 216 pp. <http://hdl.handle.net/1822/11781>

[26] Cornelissen HAW, Hordijk DA, Reinhardt HW. Experimental determination of crack softening characteristics of normal and lightweight concrete. HERON, Fracture Mechanics and Structural Aspects of Concrete 1986; 31(2):45-56.

TABLE CAPTIONS

Table 1 — Properties of the beams.

Table 2 — Mechanical properties of the CFRP laminates (average values) [15].

Table 3 — Main results obtained in the monotonic tests.

Table 4 — Main results obtained in the fatigue tests.

Table 5 — Properties adopted for the simulation of the steel reinforcements, CRFP and MDL-CFRP.

Table 1 — Properties of the beams.

Beam	Type of laminate	N.º of laminates	t_f [mm]	L_f [mm]	w_f [mm]	$\rho_{s,eq}$ [%]
REF	-	-	-	-	-	0.439
EBR	Unidirectional	2	1.41	1400	30	0.550
MF-EBR	Multidirectional	2	2.07	1400	30	0.553
NSM	Unidirectional	4	1.41	1400	15	0.561

Table 2 — Mechanical properties of the CFRP laminates (average values) [15].

Property	UD-CFRP	MDL-CFRP
Tensile strength [MPa]	2435 (CoV=5.8%)	1866 (CoV=5.1%)
Modulus of elasticity [GPa]	158 (CoV=3.9%)	118 (CoV=2.8%)
Ultimate tensile strain [%]	1.50 (CoV=4.7%)	1.58 (CoV=5.1%)
Unclamped bearing strength [MPa]	n/a	316.4 (CoV=11.8%)
Clamped bearing strength [MPa]	n/a	604.4 (CoV=5.8%)

Table 3 — Main results obtained in the monotonic tests.

Beam	Crack initiation		Yielding		Ultimate		δ_{max}/δ_y	$\varepsilon_{fy}/\varepsilon_{fu}$	$\varepsilon_{fmax}/\varepsilon_{fu}$	FRP Failure mode
	δ_{cr} [mm]	F_{cr} [kN]	δ_y [mm]	F_y [kN]	δ_{max} [mm]	F_{max} [kN]		[%]	[%]	
REF	0.36	29	3.8	70	22.6	79.3	5.95	-	-	-
EBR	0.27	25	4.1	90	7.4	108.4 (37%)*	1.80	24.0	36.6	Peeling
MF-EBR	0.38	32	4.2	96	18.3	148.2 (87%)*	4.35	15.8	69.3	Bearing
NSM	0.40	29	4.9	104	14.6	147.3 (86%)*	2.98	23.4	63.3	Rip-off

* $(F_{max} - F_{max,REF})/ F_{max,REF}$ where $F_{max,REF}$ is the maximum load of the reference beam.

Table 4 — Main results obtained in the post-fatigue monotonic tests.

Beam	Crack initiation		Yielding		Ultimate					FRP Failure mode
	δ_{cr} [mm]	F_{cr} [kN]	δ_y [mm]	F_y [kN]	δ_{max} [mm]	F_{max} [kN]	δ_{max}/δ_y	$\varepsilon_{fy}/\varepsilon_{fu}$ [%]	$\varepsilon_{fmax}/\varepsilon_{fu}$ [%]	
REF	0.26	20	2.5	66	23.3	79.9	9.32	-	-	-
EBR	0.32	27	3.0	94	7.1	114.2 (43%)*	2.37	14.6	29.6	Peeling
MF-EBR	0.35	31	3.7	101	12.9	147.2 (84%)*	3.49	15.0	63.4	Bearing
NSM	n/a	n/a	3.3	105	22.2	160.7 (101%)*	6.73	15.4	55.7	Rip-off

* $(F_{max} - F_{max,REF})/ F_{max,REF}$ where $F_{max,REF}$ is the maximum load of the reference beam.

Table 5 — Properties adopted for the simulations of the steel reinforcements, UD-CRFP and MDL-CFRP.

Material	ε_{P1} [‰]	σ_{P1} [MPa]	ε_{P2} [‰]	σ_{P2} [MPa]
Ø6	2.36	452.0	135.75	475.00
Ø10	2.53	455.0	160.00	475.00
UD-CFRP	15.00	2434.6	-	-
MDL-CFRP	3.30	390.0	20.00	850.00

Note: bi-linear law defined by the points (ε_{P1}, σ_{P1}) and (ε_{P2}, σ_{P2}). ε_{P1}=strain at the end of the first branch; σ_{P1}=stress at the end of the first branch; ε_{P2}=strain at the end of the last branch; σ_{P2}=stress at the end of the last branch.

FIGURE CAPTIONS

Fig. 1 — RC beam: (a) cross section; (b) longitudinal view. Note: all dimensions are in millimetres.

Fig. 2 — Cross section of the strengthened beams: (a) EBR; (b) MF-EBR; (c) NSM. Note: all dimensions are in millimetres.

Fig. 3 — Test configuration: (a) vertical deflection; (b) strains on the steel bars; (c) strains on the laminate of the EBR beam; (d) strains on the laminate of the MF-EBR beam; (e) strains on the laminates of the NSM beam. Note: all dimensions are in millimetres.

Fig. 4 — Force *vs*. displacement relationship of the tested beams under monotonic loading.

Fig. 5 — Failure mode of the MDL-CFRP laminates in the MF-EBR strengthened beam: (a) lateral view; (b) bearing failure detail of the laminates.

Fig. 6 — Strain variation in the FRPs.

Fig. 7 — Failure mechanisms in the MF-EBR beam.

Fig. 8 — Force *vs*. displacement relationship of the beams after the fatigue cycles.

Fig. 9 — Variation of the displacement at mid-span along the fatigue cycles.

Fig. 10 — Geometry, the finite element mesh, loading and support conditions of the MF-EBR beam. Note: all units are in millimetres.

Fig. 11 — Load *vs*. deflection at mid-span obtained experimentally and numerically for the monotonic tested beams.

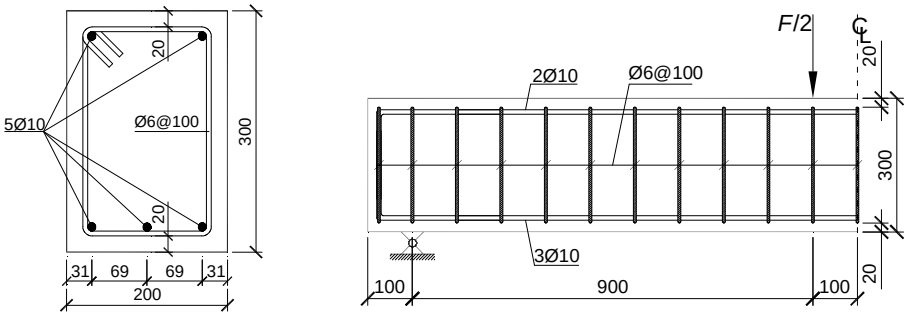

(a) **(b)**

Fig. 1 — RC beam: (a) cross section; (b) longitudinal view. Note: all dimensions are in millimetres.

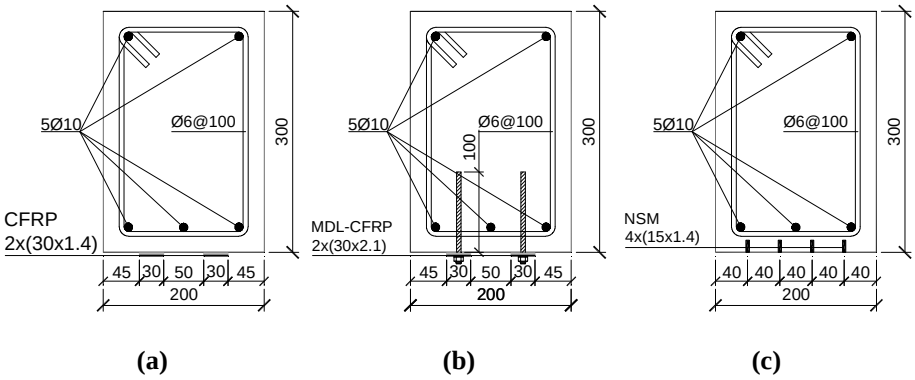

Fig. 2 — Cross section of the strengthened beams: (a) EBR; (b) MF-EBR; (c) NSM. Note: all dimensions are in millimetres.

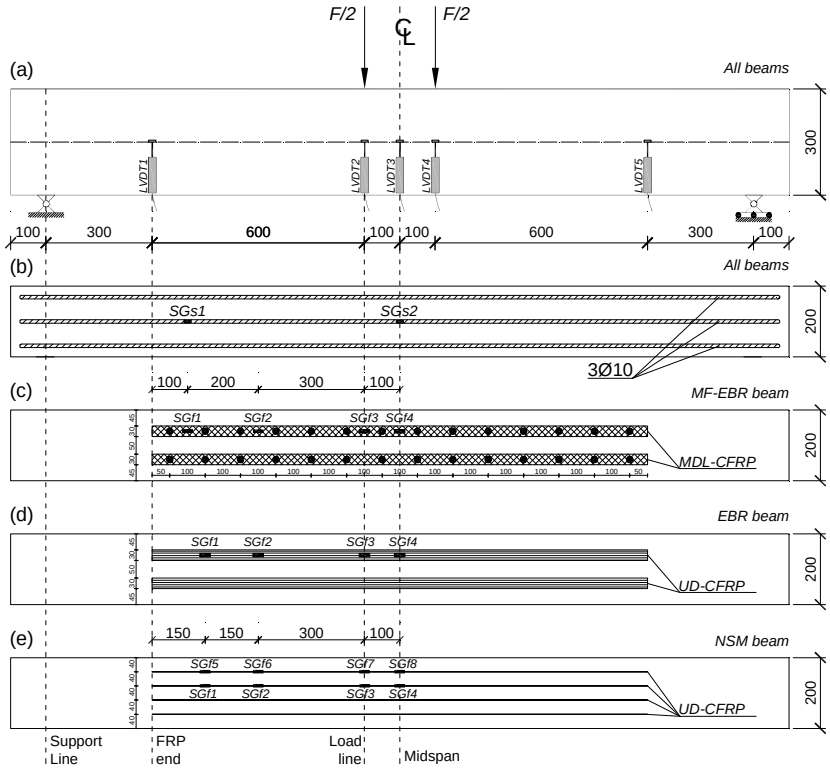

Fig. 3 — Test configuration: (a) vertical deflection; (b) strains on the steel bars; (c) strains on the laminate of the EBR beam; (d) strains on the laminate of the MF-EBR beam; (e) strains on the laminates of the NSM beam. Note: all dimensions are in millimetres.

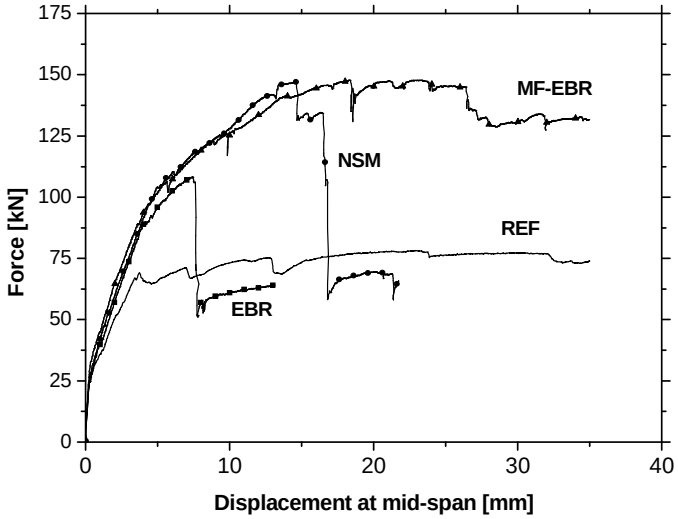

Fig. 4 — Force *vs.* displacement relationship of the tested beams under monotonic loading.

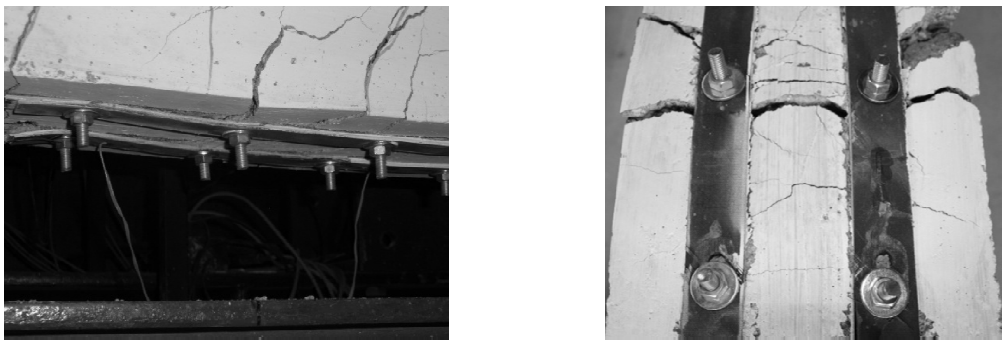

(a) (b)

Fig. 5 — Failure mode of the MDL-CFRP laminates in the MF-EBR strengthened beam: (a) lateral view; (b) bearing failure detail of the laminates.

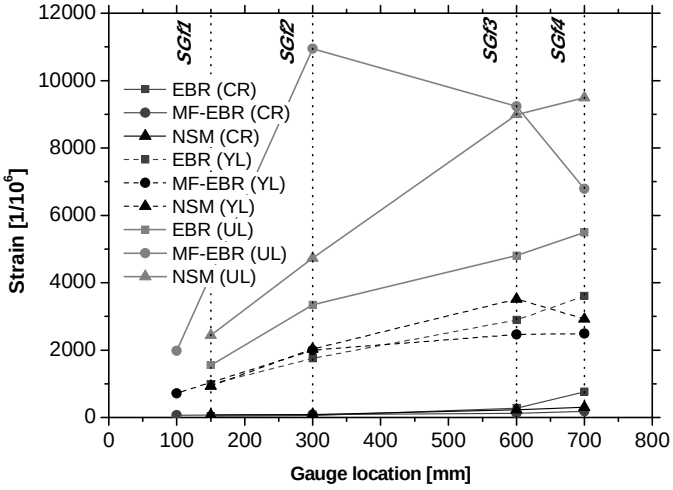

Fig. 6 — Strain variation in the FRPs.

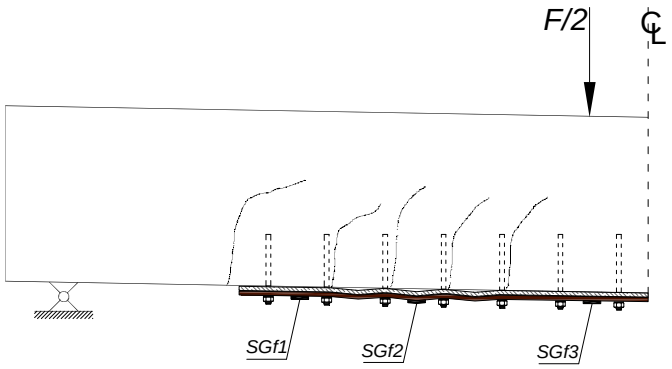

Fig. 7 — Failure mechanisms in the MF-EBR beam.

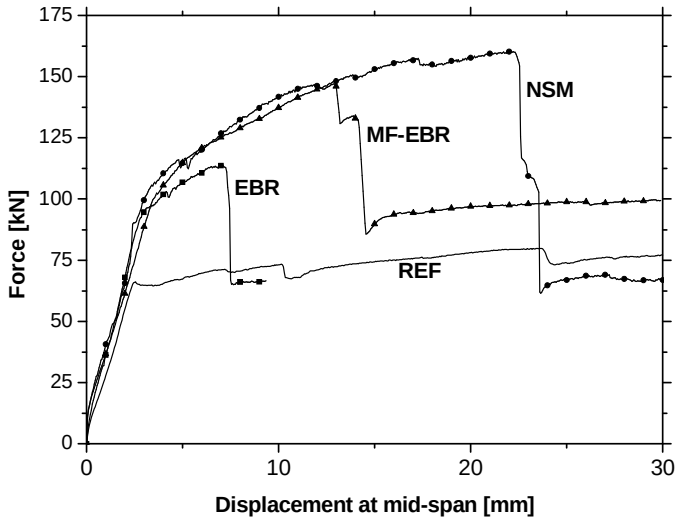

Fig. 8 — Force *vs.* displacement relationship of the beams after the fatigue cycles.

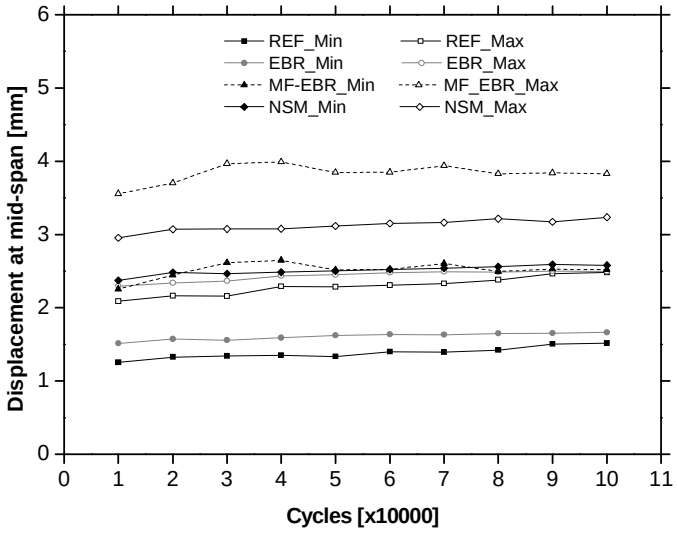

Fig. 9 — Variation of the displacement at mid-span along the fatigue cycles.

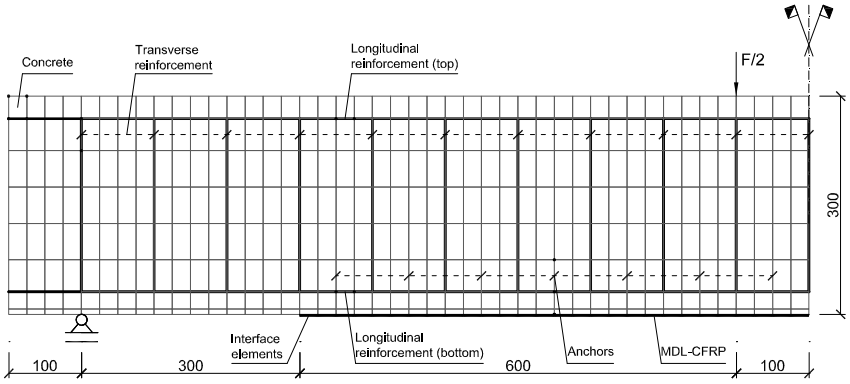

Fig. 10 — Geometry, finite element mesh, and loading and support conditions of the MF-EBR beam.

Note: all units are in millimeters.

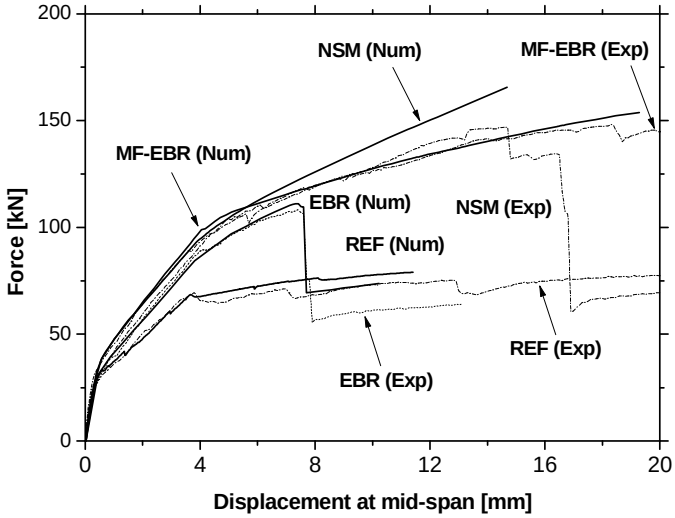

Fig. 11 — Load *vs*. deflection at mid-span obtained experimentally and numerically for the monotonic tested beams.